E-Glass/DGEBA/*m*-PDA Single Fiber Composites: New Insights into the Statistics of Fiber Fragmentation

JAEHYUN KIM,[1] STEFAN LEIGH,[2] GALE HOLMES[1]

[1]Polymers Division, National Institute of Standards and Technology, Gaithersburg, Maryland 20899-8541

[2]Statistical Engineering Division, National Institute of Standards and Technology, Gaithersburg, Maryland 20899-8980

Received 8 December 2008; revised 8 July 2009; accepted 27 July 2009
DOI: 10.1002/polb.21818
Published online in Wiley InterScience (www.interscience.wiley.com).

ABSTRACT: The interfacial shear strength is a critical parameter for assessing composite performance and failure behavior. This parameter is usually obtained from a single-fiber fragmentation test that induces sequential fracture with increasing strain of a single embedded fiber with output being the distribution of fragment lengths. An exact analytical form for the expected fragment length distribution is still not known. Such data are often fit empirically to Weibull, shifted-exponential, or lognormal distribution functions. In this report, new insights into the sequential fiber fracture process are provided by detailed analyses of the fiber break locations along the length of the embedded fiber. From this approach, the high degree of uniformity of the break coordinate loci strongly suggests that there can be no mechanistic rationale for the use of the Weibull, or lognormal, or exponential functions to fit the fragment lengths. © 2009 Wiley Periodicals, Inc. J Polym Sci Part B: Polym Phys 47: 2301–2312, 2009

Keywords: composites; failure; fragmentation; glass fibers; interface; mechanical properties; polymer-matrix composites (PMCs); uniform spacings

INTRODUCTION

The single-fiber fragmentation test (SFFT) involves the continuous or sequential straining of a single-fiber embedded in a dogbone-shaped matrix that has a strain-to-failure three to four times the fiber's strain-to-failure [i.e., a single-fiber composite (SFC)] (Fig. 1).[1] The raw data outputs from the SFFT are obtained by forcing the embedded fiber in the SFC to break under tensile load into smaller fragments without nucleating a critical flaw that causes the failure of the host matrix. The data from the SFFT formally consists of a record of the location of each break along the length of the embedded fiber and the stress and strain at which that failure occurred, with the objective being to use this data to determine the critical stress transfer length (l_c), where $l_c/2$ is the length required to transfer the applied stress to the embedded fiber, and $\sigma_f\{l_c\}$ (i.e., the strength of the fiber at l_c).[2] The data most often obtained from the SFFT is a record of how many total breaks occur over a predefined region as a function of stress or strain. These data have been shown to be reasonably accurate in determining the average fragment length at saturation, with this value being multiplied by a prefactor to obtain l_c.[3,4] Gulino and Phoenix[5] have shown that Weibull parameters obtained from single-fiber tests (SFTs) of the embedded fibers cannot be used to estimate fiber strengths on the order of l_c,

Correspondence to: G. Holmes (E-mail: gale.holmes@nist.gov)

Journal of Polymer Science: Part B: Polymer Physics, Vol. 47, 2301–2312 (2009)

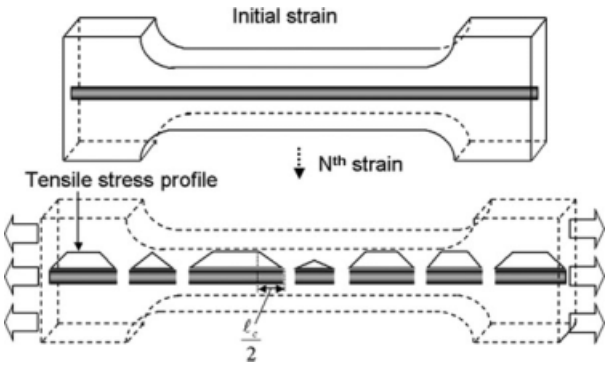

Figure 1. Schematic representation of fiber fragments occurring in the single-fiber fragmentation test.

$\sigma_f\{l_c\}$. Methodologies based on the SFFT fiber break evolution process,[2,6–8] and the fragment length distribution at saturation[9–12] have been devised to estimate $\sigma_f\{l_c\}$.

These analyses are based on the assumption that the embedded fiber contains flaws that are distributed along its length according to a spatial Poisson process and SFT data that indicate that the strength distribution of the flaws follows a Weibull distribution function.[3,13,14] Other researchers have found that below saturation the fragmentation data is better fit by a shifted-exponential distribution function.[9] In addition to the Weibull and the shifted-exponential distributions, the lognormal distribution[15] and the Gaussian distribution functions[16] have also been used to fit the final fragment length data from the SFFT. The diversity of analytical approaches indicates that there is no consensus on the distribution of fragment lengths to be expected from this test.

Theoretical approaches, where the SFFT fragmentation data have been generated by computer simulation, have also been used to investigate fragment length statistics.[2,4,6,17] However, the fit of these data depends on the type of loading assumed (i.e., Kelly-Tyson or shear-lag), with some researchers suggesting that the fragment length data are best fit by a two component model that includes Weibull and exponential distribution functions.

Recently, researchers[18–22] have sought to overcome the difficulties of extracting interfacial shear strength values from the SFFT by incorporating the number of breaks that occur at a given stress or strain level in a numerical simulation, the intent being to obtain interfacial shear strength values by adjusting the parameters of the numerical simulation until the experimental data is matched. In the most recent discussions[20–22] of this procedure the triethylenetetraamine (TETA) cured diglycidyl ether of bisphenol-A (DGEBA) matrix is modeled as isotropic elastic-plastic with linear isotropic hardening, rather than nonlinear viscoelastic. Research[23] has shown that the testing rate can affect the number of fiber breaks obtained in some resin formulations. More important, however, is that the numerical analysis process is complicated by the DGEBA/TETA matrix exhibiting matrix cracks at intermediate and high interfacial shear strengths.

Therefore, the key questions that emerge from the literature are: (1) What is the expected distribution of the fragment lengths at saturation? (2) Does this distribution remain the same throughout the break evolution process (i.e., as the stress or strain is increased)? and (3) What are the physics of the sequential fragmentation process?

In contrast to research that has focused primarily on empirically fitting the fragment lengths at saturation to various candidate distributions, this article investigates the distribution of the fiber break coordinates at successive strain increments during the test. Secondly, the matrix and the bare (unsized) E-glass fibers used in this study simplify the complex stress fields surrounding the fiber break region. This is accomplished by suppressing the formation of matrix cracks,[18–22] while maintaining a high level of adhesion between the matrix and the embedded fiber. The recording of the temporal evolution of the break locations also permits a detailed investigation of the sequential fragmentation process. The data obtained in this study also provide a basis for validating fragmentation data that can be obtained from a newly developed automated fiber fragmentation testing machine that uses digital images to archive the data from single-fiber and multi-fiber fragmentation specimens.[24,25]

EXPERIMENTAL

In this article, bare (unsized) E-glass fibers embedded in an epoxy resin composed of the DGEBA and *meta*-phenylenediamine (*m*-PDA) were tested using the SFFT methodology. Consistent with data on E-glass SFCs made of DGEBA cured with 1,2-diaminocyclohexane,[26] fracture of the bare E-glass fibers in the DGEBA/*m*-PDA matrix resulted in interfacial debonding (<4% of the total fiber length) with no matrix crack formation. In contrast with data published by others, the break

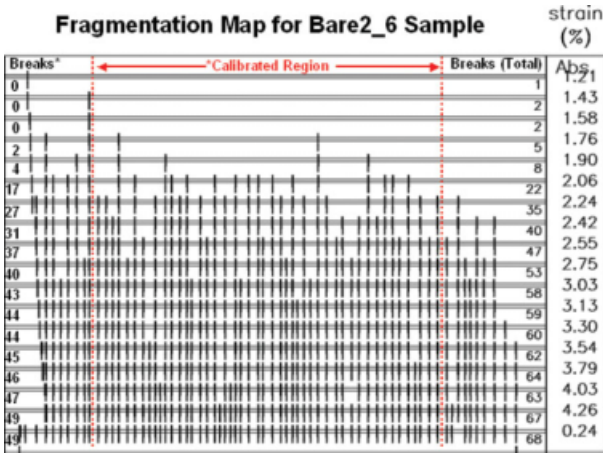

Figure 2. Fragmentation map for bare E-glass/DGEBA/*m*-PDA SFFT specimen tested by the slow test protocol. Due to limitations of the linear variable differential transducer, accurate fiber coordinates were measured only between the dashed lines (the calibrated region). The numbers of fiber breaks in this calibrated region are indicated on the left side of the figure with the corresponding strains on the right side. [Color figure can be viewed in the online issue, which is available at www.interscience.wiley.com.]

locations are recorded at each strain level and also at the end of the test in the unstressed state. Specimens containing single embedded fibers were tested using two different protocols whose representative load-time curves have been previously published.[23,27]

In the cited reports, fast and slow test protocols consisting of approximately equal strain increments spaced 10 min apart and 1 h apart were used to apply uniform deformation increments to the test specimens. Since there was not sufficient time between strain increments to measure the fiber breaks with the fast test protocol, an intermediate or variable test protocol was also implemented to examine the impact of the shorter dwell time on the fragmentation process. These specimens were loaded at 10 min intervals between strain increments until the occurrence of the first break. The time between subsequent strain increments was then increased to the time required to manually record all of the break locations. These detailed data permit the quantitative analysis of the break evolution process with increasing stress. In this report, the data from the intermediate and slow test protocols are evaluated. Additional details of the specimen test procedure and sample preparation may be found in previous publications.[23,27]

RESULTS AND DISCUSSIONS

Evolution of Fiber Break Spacing

One way to examine the results of the SFFT experiments is a fragmentation map (Fig. 2). This display shows a schematic of the fiber measurement section at each strain step with the locations of the individual breaks marked. The pictures start at the end of the first step where at least one break is found and continue until saturation is reached. After the first schematic, each picture is compressed along the horizontal axis so that the corresponding flaws align vertically. From the strain in the first picture and the compression for each subsequent picture, the specimen strain at each increment can be calculated, as shown along the right margin of the plot. The final schematic (at the bottom) is for the sample after the load was removed, and the specimen was allowed to recover for at least 24 h. The residual strain (0.24%) represents long-term or permanent deformation. The strain values obtained by the program are supported by direct strain measurements

Table 1. Fiber Break Count, Calibrated Lengths and Average Fragment Lengths for Bare Specimens

Specimen	Fiber Break Count		Calibrated Region Length (μm)	Average Fragment Length (μm)	
	Total	Calibrated Region		Total Breaks	Calibrated Breaks
Bare2_1	71	42	16,124.2	362.9	393.3
Bare2_2	69	45	16,305.8	373.5	370.6
Bare2_3	71	42	16,109.9	362.9	392.9
Bare2_5	67	40	16,350.4	384.8	419.2
Bare2_6	78	49	16,117.1	329.9	335.7
Bare2_7	76	49	16,242.3	338.7	338.4
Bare2_9	72	46	16,272.0	357.7	361.6
Bare2_10	76	50	16,204.0	338.7	330.7

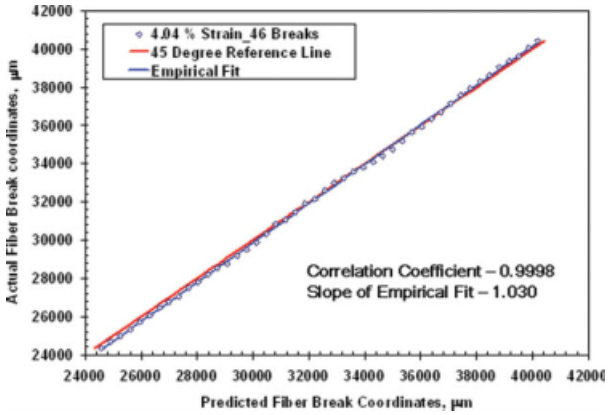

Figure 3. Uniform probability plot of fiber break coordinates for Bare2_6 test specimen at 4.04% strain. The predicted fiber break coordinates are obtained from uniform median order statistics.

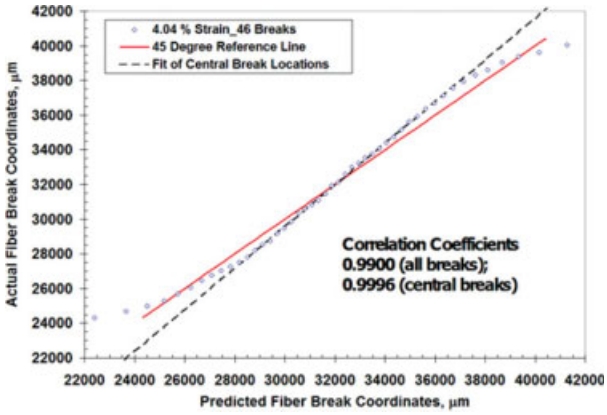

Figure 4. Weibull probability plot of fiber break coordinates for Bare2_6 test specimen at 4.04% strain. The ideal fit is obtained by taking the actual fiber break coordinates to be equal to the predicted fiber break coordinates.

from the fiducial marks that were placed on the specimen before testing.

Consistent with St. Venant's principle, only the fiber breaks in the central 16 mm part (calibrated region) of the 25.4 mm gage length test specimen were analyzed. In Table 1, the data indicate that the impact of the grips on the fragmentation behavior in the excluded region is dependent on the testing protocol. In previous analyses of the data,[27] it was shown that the number of fiber breaks at saturation for specimens tested by the intermediate protocol are less than the number of breaks for specimens tested by the slow protocol. In addition, the average fragment lengths were found to be statistically different between these two test protocols at strain levels well below the saturation strain.

Distribution of Fiber Break Coordinates

The spatially ordered fiber break coordinates were tested for goodness-of-fit of different distributions using probability plotting. Sorted sample values are plotted against scaled theoretical predictions of sample elements for the given sample size conditioned on the distribution test choice: exponential, Weibull, etc. Goodness-of-fit is judged by the straightness of the plotted pairs (theoretical, empirical) of points, quantifiable by correlation (probability plot correlation coefficient (ppcc)).

An example of a uniform probability plot of the fiber break coordinates at saturation in the unstressed state is shown in Figure 3. Irrespective of testing protocol, the fiber break coordinates in all of the specimens in Table 1 were found to conform to a uniform distribution at saturation, with a minimum ppcc across all specimens tested of 0.9985. This means that the break coordinates tend strongly to be stochastically equally spaced along the fiber. The consistently high uniform correlations suggest that there is no preferential siting of breaks: all break locations are equiprobable. In this figure, the actual break point coordinates when plotted against the uniform predicted coordinates agree very well, with a slope of 1.030 and a correlation coefficient of 0.9998.

For comparison, the fiber break coordinates were also fit to the 2- and 3-parameter Weibull functions. Correlation coefficients of 0.965 and

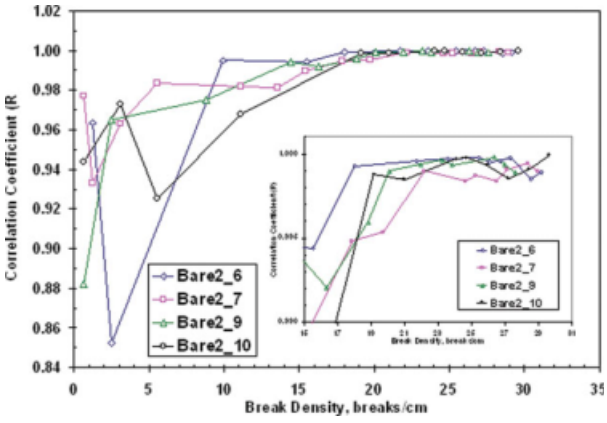

Figure 5. Evolution of probability plot correlation coefficients of fiber break locations versus break density, assuming a uniform distribution. Specimens tested by slow test protocol. Lines are drawn to facilitate interpetation. Insert emphasizes detail in the break density range of 15–31 breaks/cm.

0.990 were obtained, respectively. A plot of the 3-parameter Weibull fit is shown in Figure 4. The plot of the actual fiber break coordinates relative to the Weibull predicted coordinates, however, displays a sigmoidal shape consistently across all data sets, indicative of an underlying distribution shorter tailed than the Weibull. Correlation for the Weibull comparable to that of the uniform in Figure 3 is obtained by restricting the fit to the central 10 mm region of the 25.4 mm gage length.

Figure 5 shows the evolution of the uniform probability plot correlation coefficients for the slow test protocol with increasing break density. Similar results were obtained for specimens tested by the intermediate test protocol. The initial high correlation coefficients observed in some of the specimens are due to a random chance that the initial 4 or 5 weak flaws are spaced properly to yield uniformly spaced fracture sites. The initial high correlations generally decrease with an increasing number of breaks, suggestive of additional stochastic fracture. Above 10 breaks/cm, however, the distribution of the fiber break coordinates evolves consistently to a uniform distribution that is fully achieved at (17 to 18) breaks/cm. For all specimens tested the ppcc continues to increase until saturation is reached at approximately (22–26) breaks/cm.

Physically, the uniform distribution of fiber break coordinates means that there is no preferential location along the axis of the embedded fibers for a new break to occur. As a result of this uniform distribution of breaks, all spatial distributions of interest are dictated mathematically by the theory of Uniform Spacings. Uniform Spacings gives exact forms for many of the distributions and statistics arising from uniform breakages, including expected values, variances, covariances/correlations, and marginal and joint break coordinate and certain fragment length ("spacings") distributions.[28]

Cumulative Distribution of Fragment Lengths

In Figure 6, plots are shown of the experimental ordered fragment lengths versus expected ordered fragment lengths under a uniform distribution (see Appendix for equation). The expected values of ordered fragment lengths (spacings) obtained at saturation (27 breaks/cm) and where the break locations initially exceed a ppcc of 0.99 (16 breaks/cm) are shown for a representative SFFT specimen (designated as Bare2_9, see ref. 27) tested by the slow test protocol. For seven of the eight specimens tested, a better fit to the expected fragment lengths was obtained at the point where the correlation of fiber breaks to the uniform distribution initially increased above 0.99. Although the probability plot correlation coefficients of the break locations exhibit no decrease (Fig. 5), the reduction in the regression fit statistics of the ordered fragment lengths from 0.996 (16 breaks/cm) to 0.916 (27 breaks/cm) in Figure 6 suggests deterioration in the uniform distribution of fiber break locations.

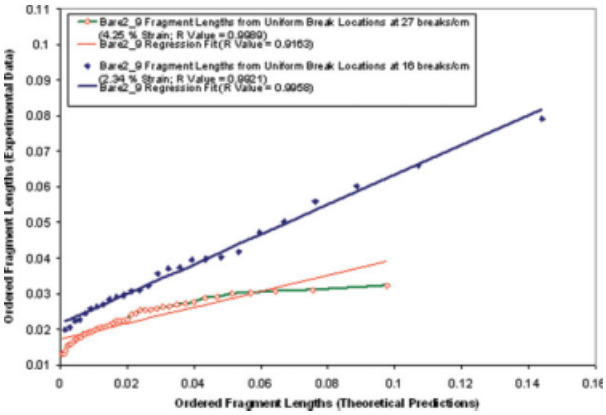

Figure 6. Plot of ordered fragment lengths from Bare2_9 SFFT specimen tested by intermediate protocol relative to the theoretical expected length values from a uniform distribution. Experimental values were taken from fragment lengths at saturation (4.25% strain, 27 breaks/cm) and the point where uniform fiber breaks were achieved (2.34% strain, 16 breaks/cm). All fragment lengths are given in the unstressed state. [Color figure can be viewed in the online issue, which is available at www.interscience.wiley.com.]

Attention is now drawn to what may be a nonrandom occurrence of fragments after the fiber break locations become uniform. A detailed analysis of the tested specimens indicates that after the distribution of fiber breaks becomes uniform (correlation greater than 0.99, Fig. 5), between (50 and 80%) of the fragments occurring are somewhat nonrandom, in that each new fragment lies between (40 and 60%) of the original parent fragment length with lengths that are within 100 μm of each other. That is, subsequent breaks tend to center between existing breaks. Before the break locations being uniform only (0–10%) of the fiber breaks conformed to this pattern.

A uniform fracture site theory is based on the occurrence of random breaks occurring along a fiber with no consideration to potential zones of low stress that arise from the transfer of stress

between the matrix and the embedded fiber as occurs in the SFFT. Therefore, it is possible that these later nonrandom fractures may limit the applicability of the uniform statistics based solutions to the regime where the fiber break locations initially achieve uniformity. As the break density increases, the accessible regions capable of fracture are clearly reduced due to the increased percentage of original fiber length that is used to transfer stress in and out of the fiber. As a result, nonrandom uniform fracture during the latter stages of the test might be expected in the SFFT. An estimate of the percentage of low stress regions as the break density increases is given in Table 2.

To illustrate the nonrandom uniform fracture finding, the evolution of the fragment lengths from the Bare2_9 specimen that occurred in the calibrated region is shown in Table 2. The numbering of the 45 fragments in the table from 13 to 57 reflects the fact that fragments 1–12 and 58–71 occurred outside the calibration region. Note that in Table 1 the total number of fiber breaks in the total gage section and calibrated region for Bare2_9 are 72 and 46, respectively. To catalog the strain and break density for each of the 45 fragments, Table 2 had to be broken into two parts with fragments 13–34 in part 1 and fragments 35–57 in part 2.

The data in this table are read from left to right with the unbroken fiber over the calibrated range indicated by the value of 16,272 μm at 1.69% strain. At the next strain increment (1.87% strain), the fiber breaks into two pieces, one of length 607 μm and the second of length 15,665 μm. The largest fragment breaks at the next strain increment into four daughter fragments[29] of 3057, 3180, 2435, and 6993 μm. The wide spacing between successive daughter fragments indicates that they eventually fracture into smaller pieces.

Note that the smaller 607 μm fragment does not fracture again until 3.55% strain, where it breaks into two pieces of approximately equal length (i.e., 302 and 305 μm). Because these fragments occur after the initial onset of uniform fiber break spacing that occurred at 2.34% (break density of 16 breaks/cm), these fragment pieces along with the 16 additional fragment pieces that occurred between 2.45 and 4.25% strain are highlighted in bold. Observe also that the parent fragments of 646, 603, and 580 μm also fractured at the 3.55% strain yielding nearly equal length fragments (highlighted in bold).

Eighteen additional fragment lengths were generated between 2.45 and 4.25% strain by 18 fracture events. Of these 18 events only five generated, by the above criteria, random daughter fragments. Three of these events occurred at the 2.45% strain increment where 1287, 1073, and 681 μm fragments that existed at the 2.34% strain increment fractured. The fracture of the 642 μm fragment at 2.93% strain and the fracture of the 722 μm fragment at 3.13% strain account for the remaining two random fractures. In contrast to the occurrence of 13 nonrandom fracture events after 2.34% strain (16 breaks/cm), only 1 of the 27 fragments generated up to the break density of 16 breaks/cm resulted in the generation of nonrandom daughter fragments. This occurred at 2.27% strain (14.1 breaks/cm) where an 825 μm fragment fractured to generate daughter fragments of 397 and 428 μm. The occurrence of these apparently nonrandom center breaks as saturation is approached in each test specimen could be responsible for the observed reduction in the goodness-of-fits relative to the expected fragment lengths.

Distribution of Fragment Lengths at the Beginning of the SFFT

Since the fiber break locations evolve to a uniform distribution, a critical look at the early fragmentation process may provide clues to the preferred distribution at the beginning of the SFFT. From the research of Wadsworth and Spilling[30] and Wagner and Eitan,[9] it would be expected that the minimal contribution of l_c to the overall fragment lengths at the early stages of the SFFT should yield fragment lengths whose distribution is a shifted-exponential. Because of the small number of fiber breaks that occur very early in the test, the data from all the samples tested by a given testing protocol were pooled and normalized by their respective fiber diameters. The cumulative probabilities were plotted relative to the natural logarithms of the ordered fiber aspect ratios and fit by linear regression. The R-values given in Figure 7 indicate that the shifted-exponential function provides a reasonable fit to the pooled and normalized fragment length data in the case of the slow protocol, and a poor fit in the case of the intermediate protocol. The small size of each data set, the generation of weak flaws resulting from handling of the fibers, and many other factors probably contributes to the variability observed in fitting these data.

Table 2. Fragment Evolution Pattern from Bare2_9 Test Specimen

Break density, breaks/cm	0	0.6	2.5	8.6	14.1	16.0	18.4	19.7	21.5	22.7	23.4	25.8	25.8	26.4	27.0
% Transfer length	2.2	4.4	11.1	33.3	53.3	60.0	68.9	73.3	80.0	84.4	86.7	95.6	95.6	97.8	100
Number of fragments	1	2	5	15	24	27	31	33	36	38	39	43	43	44	45
% Strain	1.69	1.87	1.99	2.15	2.27	2.34	2.45	2.63	2.93	3.13	3.35	3.55	3.75	3.94	4.25
Fragment no.															
13	16,272	607	607	607	607	607	607	607	607	607	607	**302**	302	302	302
14												**305**	305	305	305
15		15,665	3,057	646	646	646	646	646	646	646	646	**334**	334	334	334
16												**312**	312	312	312
17				868	506	506	506	506	506	506	506	506	506	506	506
18					363	363	363	363	363	363	363	363	363	363	363
19				462	462	462	462	462	462	462	462	462	462	462	**213**
20															**249**
21				642	642	642	642	642	**415**	415	415	415	415	415	415
22									**227**	227	227	227	227	227	227
23				438	438	438	438	438	438	438	438	438	438	438	438
24			3,180	1,084	1,084	603	603	603	603	603	603	**343**	343	343	343
25												**259**	259	259	259
26						482	482	482	482	482	482	482	482	**267**	267
27														**214**	214
28				2,096	681	681	**287**	287	287	287	287	287	287	287	287
29							**394**	394	394	394	394	394	394	394	394
30					835	499	499	499	499	499	499	499	499	499	499
31						336	336	336	336	336	336	336	336	336	336
32					580	580	580	580	580	580	580	**253**	253	253	253
33												**327**	327	327	327
34			2,435	370	370	370	370	370	370	370	370	370	370	370	370
35				825	397	397	397	397	397	397	397	397	397	397	397
36					428	428	428	428	428	428	428	428	428	428	428
37				474	474	474	474	474	474	474	474	474	474	474	474
38				766	766	766	**413**	413	413	413	413	413	413	413	413
39							**353**	353	353	353	353	353	353	353	353
40			6,993	3,084	979	979	979	979	**491**	491	491	491	491	491	491
41									**488**	488	488	488	488	488	488
42					1,287	1,287	**566**	566	**278**	278	278	278	278	278	278
43									**288**	288	288	288	288	288	288
44							**722**	722	722	**412**	412	412	412	412	412
45										**309**	309	309	309	309	309
46					817	817	817	**366**	366	366	366	366	366	366	366
47								**451**	451	451	451	451	451	451	451
48				1,566	911	911	911	**468**	468	468	468	468	468	468	468
49								**443**	443	443	443	443	443	443	443
50					655	655	655	655	655	655	**317**	317	317	317	317
51											**339**	339	339	339	339
52				2,343	1,073	1,073	**280**	280	280	280	280	280	280	280	280
53							**793**	793	793	**364**	364	364	364	364	364
54										**429**	429	429	429	429	429
55					946	526	526	526	526	526	526	526	526	526	526
56						420	420	420	420	420	420	420	420	420	420
57					324	324	324	324	324	324	324	324	324	324	324

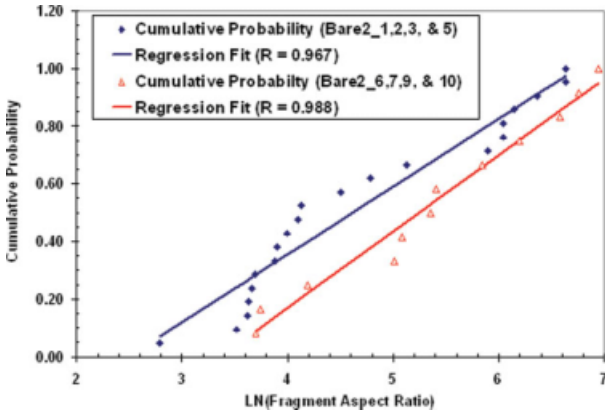

Figure 7. Cumulative probability plot versus the natural logarithm of the fragment aspect ratios for fragment lengths occurring very early in the fragmentation process. The results shown in the figure are for specimens tested by the intermediate test protocol (Bare2_1,2,3 & 5) and the slow test protocol (Bare2_6,7,9, & 10). [Color figure can be viewed in the online issue, which is available at www.interscience.wiley.com.]

Comparison of E-Glass/Epoxy SFC Data with Single-Fiber Composite Theories

The fiber break evolution data provided in Table 2 provide a unique opportunity to compare the experimental results from the E-glass SFCs investigated in this report to the the two "exact" theories for the SFC test that were developed by Curtin[2] and Phoenix and coworkers[6] in the early to mid 90s. These theories are supported by the experimental data of Gulino et al.[31] who reportedly obtained fiber break location data on two different carbon fiber micro-composite specimens, where the 5.5 μm graphite fiber was sandwiched between two 13 μm SK glass fibers with an inter-fiber distance of (3 $\pm$ 1) μm along the specimen length. Their data indicate maximum break densities (25 and 14.5 breaks/cm) that are in the range observed in this report. Furthermore, their plots of the evolution of the break density with fiber composite stress conformed to a Weibull distribution at saturation. Curtin, however, found it difficult to understand why the distribution of breaking stresses should follow a Weibull form over such a wide range of stresses.

These experimental data along with Monte Carlo simulations form the basis of the two exact theories, under the key assumption that the host matrix undergoes elastic perfectly plastic (EPP) deformation during the fiber fragmentation process. Holmes et al.[23] have shown that this assumption does not hold for the DGEBA/*m*-PDA matrix used here, and that fiber fragmentation occurs when the matrix is exhibiting nonlinear viscoelastic behavior. The assumed matrix behavior leads to the establishment of a critical transfer length zone, $\delta\{\sigma\}/2$, whose length depends on the current applied stress, σ. The zone also precludes additional fracture events from occurring in the region surrounding an existing fiber break. As a consequence of this assumed behavior, Curtin[2] formulated his theory by viewing the fiber fragmentation process as occurring in two parts: (i) those fragments formed by breaks separated by more than $\delta\{\sigma\}$ at the current stress level σ and (ii) those fragments smaller than δ which were formed at an earlier stress level $\sigma' < \sigma$ when a shorter $\delta\{\sigma'\} < \delta\{\sigma\}$ prevailed. Consequently, the filtered length distribution of fragment lengths in part (i) that contain all fragments larger than $\delta\{\sigma\}$ are viewed as being the same as that for a fiber with a unique strength, σ, whose effective fiber length is $L_T - L_R$, where L_T denotes the total length of the fiber and L_R represents the combined lengths of all fragments smaller than $\delta\{\sigma\}$. Phoenix and coworkers[4,6] in their theory found the filtered length distribution approach plausible, but took issue with the value of the maximum achievable packing density along the broken fiber stating that the value should be 1 rather than the value of 0.7476 used by Curtin.

Applying the filtered length distribution approach devised by Curtin to the experimental data obtained in this report, it is seen that his theory under-predicts the actual break density at fiber stresses above 1.5 GPa (Fig. 8), where the critical transfer length at saturation, obtained by multiplying the average fragment length at saturation by 4/3, was used as the criteria for removing fiber breaks. Since Phoenix and coworkers[4] have shown that the multiplier for obtaining the critical transfer length depends on the fiber Weibull modulus, the Curtin approach was recalculated by removing the actual nonbreaking fragments, with no better success at fitting the data above 1.5 GPa. Finally, the N_T-N_R factor in Curtin's formulation, where N_T denotes the total number of fiber breaks and N_R represents the number of breaks removed by L_R, was replaced by N_T-N_R-1 since the former factor accounts for the number of fragments and yields a nonzero value at zero fiber breaks. Although this approach did not provide a better fit of the data at high stress values, the revised formulation did fit the low stress data better.

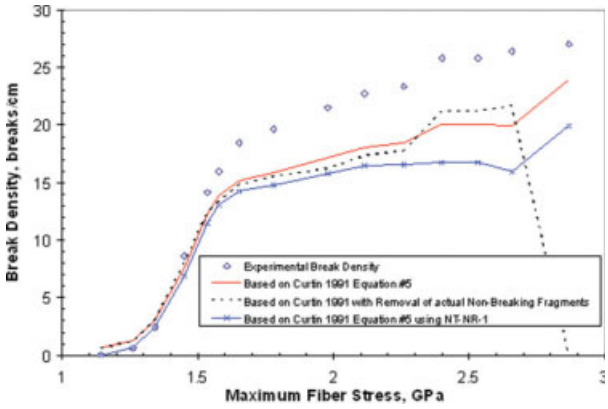

Figure 8. Comparison of break density evolution predicted by the theory of Curtin with E-glass/DGEBA/*m*-PDA SFC data. [Color figure can be viewed in the online issue, which is available at www.interscience.wiley.com.]

It is interesting to note that the filtered length distribution approach devised by Curtin and found plausible by Phoenix et al., is based on the assumption that the smallest fragments observed at saturation are formed early in the test when the critical transfer length is the shortest (i.e., the EPP assumption). The compilation of fragmentation data in Table 2 shows that the smallest fragments in the E-glass/SFC specimens tested in this report are formed at the end of the test.

Hui et al.[4] in the development of their theory expressed the break density ($\chi\{s, \rho\}$) as an exponential integral depending on the nondimensionalized stress (s) and the shape parameter (ρ) of the Weibull fiber. Since there is no closed form solution of this integral, Hui et al. provided a power-series representation of $\chi\{s, \rho\}$ valid for $s \leq 1$. Plots of this representation, the small s estimate of the data, and the closed form solution for $\chi\{s, \rho\}$ obtained by Gulino and Phoenix[5] are shown in Figure 9. From the figure, all representations for $\chi\{s, \rho\}$ provide a reasonable approximation of the experimental data for $s \leq 1$, with the Weibull parameters from all plots being obtained as prescribed by Hui et al. from the small s approximation.

The value of 18.9 for the shape parameter from the plots provided by Hui et al. [Fig. 1(a) in ref. 4] indicates that a more exact estimate of $\chi\{s, \rho\}$ would not capture the gradual rise of the break density above $s = 1$ found in our experimental data. Furthermore, this value indicates that the 4/3 multiplier used to calculate the critical transfer length in the above evaluation of Curtin's theory is appropriate for the tested E-glass fiber.

These results suggest that the theories obtained by Curtin and Hui et al. are not extendable to the E-glass fibers tested in this report, although these theories accurately model the data from three fiber micro-composites. An initial look at the three fiber micro-composite data by Gulino and Phoenix[5], shows that the break densities of (25 and 15) breaks/cm at the end of the tests were accompanied by extensive debonding on the order of (85–130 μm). In contrast, the average debond region surrounding each break at saturation in the single-fiber E-glass micro-composite analyzed for this report is less than 19 μm, with a range of 13–23 μm. This indicates that the state of stress surrounding the fiber breaks in the samples analyzed by Gulino et al. may be very different from the specimens analyzed in this report, resulting in a different fiber break and fragment evolution.

A follow-up article[32] to the results presented here indicates that the trend toward a uniform distribution of fiber breaks in the SFFT is independent of interfacial shear strength, fiber type, matrix type, and fiber-fiber interactions (at least 45 specimens evaluated). This is especially true if matrix crack formation is suppressed, as it has been in these specimens. Furthermore, the follow-up data indicates that the sizes of the fragment lengths that survive as saturation is approached decrease as the strain is increased in E-glass polyisocyanurate SFCs. Since some of these data were obtained in different laboratories associated with the last round robin testing of the SFFT, where the test specimens were all made under the auspices of the Drzal group at Michigan State

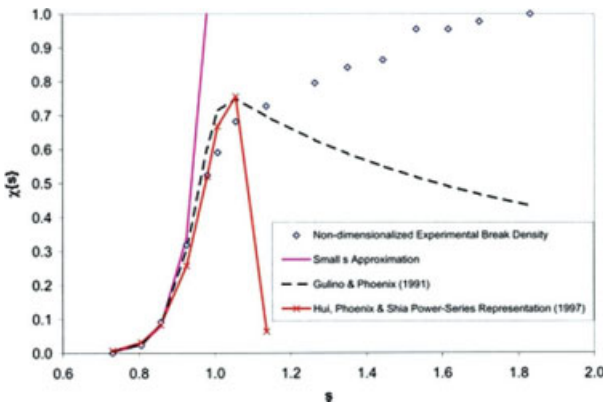

Figure 9. Comparison of break density evolution predicted by the theory of Hui et al. with E-glass/DGEBA/*m*-PDA SFC data. [Color figure can be viewed in the online issue, which is available at www.interscience.wiley.com.]

University, this suggests that the results presented in this paper are not unique to the test methodology employed in this laboratory or the bare (unsized) E-glass fibers used.

CONCLUSIONS

Analysis of the fiber break locations from SFFT specimens composed of bare E-glass fibers embedded in a DGEBA/*m*-PDA matrix cured according to the Drzal procedure[23,27] and tested by two different protocols shows that the fiber break locations at saturation conform to a uniform distribution. A detailed analysis of the break locations from each strain step shows that a uniform distribution of fiber breaks (ppcc $\geq$ 0.99) is typically achieved at (17 to 18) breaks/cm and continues to increase slightly until saturation is achieved.

The fit of the E-glass DGEBA/*m*-PDA SFC fiber break location data to a uniform distribution, although empirical, represents a departure from previous SFC results, where breaks and fragment lengths are typically fit to Weibull, lognormal, or other distributions. The considerable statistics literature about spacings (i.e., fragment lengths) derived from a uniform distribution[28,33] indicate that the ordered fragment length distribution at saturation conforms to an explicitly parameterized form obtained by Whitworth given in the appendix. Fits of break locations to a uniform distribution (ppcc $>$ 0.99) were found to be consistently better than fits of the same data to a 3-parameter Weibull distribution (ppcc $\approx$ 0.98).

The fact that a distribution form like 3-parameter Weibull seems to fit ensembles of breaks and fragment lengths from one experiment is a reflection of the fact that the Weibull is parametrically rich enough to successfully capture a wide variety of distributional shapes. But the consistent strong uniformity of the break coordinate loci and the consistent short tailedness of the Weibull probability plots show clearly that there is no mechanistic rationale for the use of the Weibull.[34]

Finally, a reviewer of this paper correctly noted that the work presented does not provide an analysis method for extracting reliable interfacial shear strength data that may be used by practitioners in the field. There have been numerous methods advanced to accomplish that task over the past 40 years with two notable theories presented as being exact[2,6] and a more recent approach based on matching numerical simulations to experimental data.[18–22]

Although matching numerical simulations to experimental data shows promise, difficulties have arisen due to the occurrence of matrix cracks associated with fiber fracture[21] and concern has been expressed by the cited researchers for validating the extracted parameters against experimental data.[19] The evolution of fiber break location data generated in this report provides a unique opportunity to determine if a simulation process that assumes the matrix to be elastic-plastic with strain-hardening captures the physics of the sequential fragmentation process. Of particular note from the research that has most recently been conducted is the observation that the sizes of the fragment lengths that survive as saturation is approached decrease as the strain is increased. Since this is the opposite of what is predicted by the elastic perfectly plastic model it would be interesting to determine if the strain-hardening introduced into the current simulation approach captures these results.

It is also interesting to note that the DGEBA/TETA matrix used for the SFCs in the numerical simulations exhibits matrix cracks when the E-glass fiber is sized or unsized,[35] whereas the bare E-glass fiber SFCs fractured in this report exhibit debonding only. The suppression of matrix cracks observed in this report are consistent with the results of Drzal and coworkers.[26] This indicates that the judicious choice of matrix may induce simplification of the failure behavior associated with fiber fracture in specimens that exhibit intermediate to high interfacial shear strength, reinforcing the applicability of the numerical simulation approach.

The authors would like to thank Professor Andrew Rukhin, University of Maryland Baltimore County/National Institute of Standards and Technology (UMBC/NIST) for his many helpful comments during the preparation of this manuscript.

APPENDIX

In testing distributional goodness-of-fit, probability plotting offers advantages over Kolmogorov-Smirnov or chi-square in that it is graphical, makes use of all the available data in its given form, and is assumption-free. Probability plots graph empirical data or quantiles against theoretical predictions based on the distribution under test. Linearity of the plot confirms goodness of fit, which can be quantified by

correlation: probability plot correlation coefficient (ppcc).[36] ppcc ≥ 0.99 indicates a good fit to the hypothesized distribution. If parameters of the distribution under test are estimated prior to plotting, the straightness of the plotted pairs relative to a 45° reference line can be used to evaluate the fit quality.

The probability plots in this paper were obtained using uniform order statistic medians as predictors of typical values from an n-fold uniform sample.[36] The formulas for computing the order statistic medians are:

$$m_1 = 1 - m_n, \qquad i = 1$$

$$m_i = (i - 0.3175)/(n + 0.365), \quad i = 2, 3, ..., n - 1,$$

where n is the sample size (here: number of breaks)

$$m_n = 0.5^{(1/n)}, \qquad i = n$$

The CDF has the form:

$$UNIF(x) = \frac{(x - a)}{(b - a)}$$

with $a \leq x \leq b$ and parameters a and b the lower and upper limits of the range. Consistent with the finite length of the tested fibers, the uniform density function (PDF) takes values over a finite range, with the probability of fracture occurring outside this region being zero and the probability within the region given by:

$$unif(x) = \frac{1}{(b - a)}, \quad b > a$$

Spacings from the uniform corresponding to the fragment lengths have properties[28,33] applicable to the fracture of fibers in SFFT and multi-fiber fragmentation test (MFFT) specimens. These include: (a) the individual spacings distribute as Beta (1, n) (n equals number of breaks), (b) the joint distributions, covariances, and correlations of pairs of spacings are all explicitly parametrizable, (c) the joint distribution of all spacings is Dirichlet, (d) the cumulative distribution of the ordered spacings follows a Whitworth distribution, and (e) there is an explicit formula for the expected value of the jth ordered spacing.

The ordered spacings (i.e., ordered fragment lengths) arising from a uniform (U[0, 1]) distribution, $D_{(1)} \leq D_{(2)} \leq ..... \leq D_{(n+1)}$, ranked from lowest to highest, have a CDF for each $D_{(n-j)}$, given by:[28,37]

$$\Pr(D_{(n-j)} \leq x) = \sum_{r=0}^{j} \binom{n}{r} \sum_{s=0}^{n-r} (-1)^s \times \binom{n-r}{s} [1 - (r+s)x]_+^{n-1},$$

where $0 < x < 1$ and $a_+ = \max(a, 0)$.

The expected size, $E(D_{(i)})$, of each ordered fragment length from a *UNIF*[0, 1] distribution can be determined solely from the total number of fiber breaks, n, using:[28]

$$E(D_{(i)}) = \frac{1}{n} \sum_{r=0}^{i-1} (n - r)^{-1}$$

It is worth noting that the uniformity of the break coordinates implicitly dictates a mathematical form for the density of the fragment lengths. This must relate to a Beta (1, n), because that is the form for the density of each individual fragment length, but the imposition of the – physical, mathematical – constraint that all the fragment lengths from any experiment must sum to the original fiber length makes the exact form of the density of fragment lengths from a single experiment very hard to parameterize explicitly.

REFERENCES AND NOTES

1. Drzal, L. T.; Herrera-Franco, P. J. In Engineered Materials Handbook: Adhesives and Sealants; Dostal, C. A.; Woods, M. S.; Ronke, A. W.; Henry, S. D.; Daquila, J. L., Eds.; ASM Int.: Metals Park, Ohio, 1990; pp 391–405.
2. Curtin, W. A. J Mater Sci 1991, 26, 5239–5253.
3. Henstenburg, R. B.; Phoenix, S. L. Polym Compos 1989, 10, 389–408.
4. Hui, C. Y.; Phoenix, S. L.; Shia, D. Compos Sci Technol 1997, 57, 1707–1725.
5. Gulino, R.; Phoenix, S. L. J Mater Sci 1991, 26, 3107–3118.
6. Hui, C. Y.; Phoenix, S. L.; Ibnabdeljalil, M.; Smith, R. L. J Mech Phys Solids 1995, 43, 1551–1585.
7. Yavin, B.; Gallis, H. E.; Scherf, J.; Eitan, A.; Wagner, H. D. Polym Compos 1991, 12, 436–446.
8. Scherf, J.; Cohen, Y.; Wagner, H. D. Int J Adhes Adhes 1992, 12, 251–256.
9. Wagner, H. D.; Eitan, A. Appl Phys Lett 1990, 56, 1965–1967.
10. Fraser, W. A.; Ancker, F. H.; Dibenedetto, A. T. Reinforced Plastics - Milestone 30; The Society

of the Plastics Industry: New York, 1975; pp 1–13.
11. Fraser, W. A.; Ancker, F. H.; Dibenedetto, A. T.; Elbirli, B. Polym Compos 1983, 4, 238–248.
12. Drzal, L. T.; Rich, M. J.; Camping, J. D.; Park, W. J. In Proceedings of the 35th Annual Technical Conference; Technomic Publishing Co.: Lancaster, Pennsylvania, 1980; pp 1–7.
13. Wagner, H. D. J Polym Sci Polym Phys 1989, 27, 115–149.
14. Netravali, A. N.; Topoleski, L. T. T.; Sachse, W. H.; Phoenix, S. L. Compos Sci Technol 1989, 35, 13–29.
15. Netravali, A. N.; Hestenburg, R. B.; Phoenix, S. L.; Schwartz, P. Polym Compos 1989, 10, 226–241.
16. Bascom, W. D.; Jensen, R. M. J Adhes 1986, 19, 219–239.
17. Ling, S. U.; Wagner, H. D. Compos Sci Technol 1993, 48, 35–46.
18. Zhao, F. M.; Okabe, T.; Takeda, N. Compos Sci Technol 2000, 60, 1965–1974.
19. Zhao, F. M.; Takeda, N. Compos A 2000, 31, 1215–1224.
20. Okabe, T.; Takeda, N. Compos A 2002, 33, 1327–1335.
21. Nishikawa, M.; Okabe, T.; Takeda, N. Mater Sci Eng A Struct 2008, 480, 549–557.
22. Nishikawa, M.; Okabe, T.; Takeda, N.; Curtin, W. A. Model Simul Mater Sci Eng 2008, 16, Article No. 055009.
23. Holmes, G. A.; Peterson, R. C.; Hunston, D. L.; McDonough, W. G.; Schutte, C. L. In Time Dependent and Nonlinear Effects in Polymers and Composites; Schapery, R. A., Eds.; ASTM: West Conshohocken, Pennsylvania, 2000; pp 98–117.
24. Holmes, G. A.; Wesson, S.; McDonough, W. G.; Kim, J. H.; Netravali, A.; Walker, J. N.; Johnson, R. J Mater Sci 2009, 44, 2007–2015.
25. Kim, J.-H.; Hettenhouser, J. W.; Moon, C. K.; Holmes, G. A. J Mater Sci 2009, 44, 3626–3632.
26. Drown, E. K.; Almoussawi, H.; Drzal, L. T. J Adhes Sci Technol 1991, 5, 865–881.
27. Holmes, G. A.; Peterson, R. C.; Hunston, D. L.; McDonough, W. G. Polym Compos 2000, 21, 450–465.
28. Read, C. B. Encyclopedia of Statistical Sciences; Kotz, S.; Johnson, N. L., Eds.; Wiley: New York, 1988; pp 566–569.
29. Holmes, G. A.; Peterson, R. C.; Hunston, D. L.; McDonough, W. G. Polym Compos 2007, 28, 561–574.
30. Wadsworth, N. J.; Spilling, I. Br J Appl Phys J Phys D 1968, 1, 1049–1058.
31. Gulino, R.; Schwartz, P.; Phoenix, S. L. J Mater Sci 1991, 26, 6655–6672.
32. Holmes, G.; Kim, J. H.; Leigh, S. D.; McDonough, W. G. J Appl Polym Sci 2008, accepted for publication 12/11/2008.
33. Pyke, R. J Roy Stat Soc B Met 1965, 27, 395–436.
34. Buckland, W. R. Statistical Assessment of The Life Characteristic: A Bibliographic Guide; 1st ed.; Hafner Publishing Company: New York, 1964.
35. Zhao, F. M.; Takeda, N. Compos A 2000, 31, 1203–1214.
36. Filliben, J. J. Technometrics 1975, 17, 111–117.
37. Holst, L. J Appl Probab 1980, 17, 623–634.